Organic Geochemistry 195 (2024) 104832

Contents lists available at ScienceDirect

Organic Geochemistry

journal homepage: www.elsevier.com/locate/orggeochem

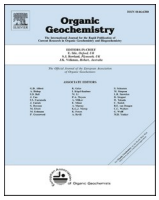

The preservation of photosynthetic and hydrological signals in the carbon and hydrogen isotope compositions of *n*-fatty acids in the seasonal wetland soils of the Okavango Delta (Botswana)

Julie Lattaud [a,*], Mangaliso J. Gondwe [b], Matthias Saurer [c], Carole Helfter [d], Cindy De Jonge [a]

[a] Biogeoscience Group, Geological Institute, ETH Zurich, Sonneggstrasse 5, Zurich, Switzerland
[b] Okavango Research Institute (ORI), University of Botswana, Sexaxa, Shorobe Rd., Maun, Botswana
[c] Swiss Federal Institute for Forest, Snow and Landscape Research, WSL, Zürcherstrasse 111, Birmensdorf, Switzerland
[d] UK Centre for Ecology and Hydrology, Library Ave, Bailrigg, Penicuik EH26 0QB, UK

ARTICLE INFO

Associate Editor — N. Pedentchouk

Keywords:
Okavango Delta
Hydrogen isotope
N-fatty acid
Carbon isotope
Plant isotopes fractionation

ABSTRACT

The Okavango wetland (Botswana) is the world's largest inland delta. A strong seasonality in water input leads to the contraction and extension of wetlands in the floodplains. The extreme evapotranspiration and little precipitation lead to a difference in the hydrogen isotope signature of rain, soil and river water. Biomarkers, such as plant waxes, are stored in the soils and preserved on geological timescales. To understand which signal is preserved in the stable isotope signatures of plant waxes, soils along a 250 m-long transect spanning waterlogged to dry soils were collected over several seasons and three years. In addition, plants, and plant and soil water were collected along this transect. First, carbon isotope ratios ($\delta^{13}C$) of plant waxes (i.e, *n*-fatty acids) were used to classify their metabolism. $\delta^{13}C$ of bulk organic matter and individual *n*-fatty acids analyzed in the soils show a strong dependance on the type of vegetation found along the transect (C_3 versus C_4 plants). Hydrogen isotope ratios (δ^2H) of water present in soil showed that shallow-rooted C_4 grasses use superficial soil water, whereas the xylem water δ^2H content in trees growing near the flooded channel indicated the use of river water. In addition, plant hydrogen fractionation between lipids and rain showed a strong influence of carbon metabolisms with larger fractionation for C_3 plants compared with C_4 grasses. *n*-fatty acid δ^2H ratios in surface soils followed the hydrological variation in the Delta with its floods and dry periods. Hence δ^2H of long-chain fatty acids seems to track the river-level variation rather than precipitation.

1. Introduction

Being able to accurately know the drivers and extent of climate change through time and in different regions is important to correctly forecast future climates. To reconstruct the amount of continental rainfall, multiple proxies exist such as lake paleo-shore analysis (e.g., Burrough et al., 2007), cellulose oxygen isotope signatures from tree rings (e.g., Saurer et al., 1997) and hydrogen isotopes (δ^2H) of plant waxes (*n*-alkanes and *n*-alkyl fatty acids (FA)), which persist in soils and geo-archives (e.g., Sachse et al., 2012). As they grow, plants incorporate hydrogen from environmental water into their leaf waxes (e.g., Sachse et al., 2012). Most plants do not capture precipitation directly but tap into soil water, hence, the isotopic signature of plant source water is determined by the soil water isotope profile (Dawson and Ehleringer, 1991; Ehleringer and Dawson, 1992; Snyder and Williams, 2000). Soil water can be ^2H-enriched compared with rain water due to evaporation, this process decreases with soil depth (Dawson and Ehleringer, 1991; Ehleringer and Dawson, 1992). In arid environments, C_3 plants tend to use ^2H-depleted rainwater, or groundwater, while C_4 plants with shallower roots use ^2H-enriched soil water (Feakins and Sessions, 2010; Schwab et al., 2015). However, in some settings where vegetation has changed recently that might not be the case (Krull et al., 2006). As such, when reconstructing paleo-hydrology using δ^2H_{wax}, a good identification of the source water is crucial. Usually, the isotopic signature of xylem water is considered equal to that of the source water used by the plant because there is no isotope fractionation during water uptake by the roots (Ehleringer and Dawson, 1992) and as such xylem water can be a proxy for the original source water. Once the plant has transported the

* Corresponding author at: Department of Environmental Sciences, University of Basel, Switzerland.
E-mail address: Julie.lattaud@unibas.ch (J. Lattaud).

https://doi.org/10.1016/j.orggeochem.2024.104832
Received 28 November 2023; Received in revised form 28 June 2024; Accepted 3 July 2024
Available online 6 July 2024

water along its stem to the leaves, transpiration via the leaves results in further isotopic enrichment of leaf water compared to xylem water (e.g., Feakins and Sessions, 2010; Griepentrog et al., 2019). This leaf water is the immediate source of hydrogen for the biosynthesis of leaf-waxes, which are strongly ^{2}H-depleted compared to leaf water due to further isotope fractionation by biochemical processes (Sachse et al., 2012). This hydrogen isotopic fractionation during biosynthesis has been shown to widely vary among plant species and growth form (e.g., −110‰ to −260‰, e.g., Sessions et al., 1999; Krull et al., 2006; Hou et al., 2007; Gao et al., 2014; Liu et al., 2016; Freimuth et al., 2017). The fractionation between source water (soil water, river water, groundwater) δ^{2}H and plant waxes δ^{2}H is called net fractionation (ε_{net}), while apparent fractionation (ε_{app}) represents the fractionation between rain water and FA. The latter encompasses all sources of uncertainty when interpreting sedimentary plant waxes δ^{2}H to reconstruct paleohydrology (e.g., Sachse et al., 2012). ε_{app} has been shown to also vary with plant growth form (Griepentrog et al., 2019), latitude (Daniels et al., 2017), aridity, and plant ecology (Douglas et al., 2012).

Constraining the ε_{app} in southern African ecosystems is relevant as (past) changes in rainfall variability across Africa are poorly understood, especially for southern Africa (e.g., Singarayer and Burrough, 2015; Chevalier et al., 2021). The current rainfall regime in southern Africa with strict seasonal rainfall zones, i.e., precipitation predominantly during the austral summer, was likely more complicated in the past (Burrough and Thomas, 2013; Thomas, 2019). Hence, building robust hydroclimatic tools to use on geological timescales is essential. The Okavango Delta wetlands, one of the world's largest inland deltas in northern Botswana, are a sensitive tracer of the balance between precipitation and evaporation. Flooding of the delta occurs in winter (June to August) (Gieske, 1997; Gumbricht et al., 2004; McCarthy and Ellery, 1998; Milzow et al., 2009). Because of the strong seasonality of water supply, this region is uniquely suited to the study of the impact of changes in source water and vegetation type across a small spatial extent and test the potential of δ^{2}H of plant waxes to trace rainfall or river water variability.

In this study we analysed plant tissue water from 16 plants (15 different species), and soil water along a soil moisture transect extending from the permanently dry inland of Chief's Island (19°32′53″S; 23°10′45″E) to the edge of the river channel, as well as FA in 43 soil samples along the transect (Fig. 1). We investigated ε_{app} in the Okavango Delta with the aim of creating a calibration framework for the region for interpreting δ^{2}H of plant waxes in paleo-hydrological reconstruction. To achieve this, we traced the carbon and hydrogen isotopic composition of plant-derived and microbe-derived FA from production in modern plants to deposition in soils and comparing these δ^{2}H of plant waxes values with isotopic observations of precipitation, river, soil and plant (xylem and leaf) waters.

2. Materials and methods

2.1. Study site, soil and plant material

Chiefs Island is the largest island in the Okavango Delta and its southern part is bordered by a seasonal floodplain area, which means that the nearby Boro channel will thus be almost completely dry during the summer months (Fig. 1). Water table depth on the island increases with distance from the channel such that the depth increases from 150 cm to 330 cm from 10 m to 40 m away from the channel (Bauer-Gottwein et al., 2007; Lubinda, 2012). In the Okavango Delta, the vegetation exhibits marked zonation, with aquatic grasses such as *Vossia cuspidata* in primary channels, which are typically flanked by *Cyperus papyrus*. The backswamp areas present a mosaic of submerged and emerged species such as *Ottelia ulvifolia*, *Najas pectinate*, *Nymphaea caerulea*, and *N. lotus*. The vegetation distribution in the seasonal swamps reflects the length of the flooding period: areas with relatively long flooding periods may have submerged and emerged species similar to the permanent swamp, while area flooded for shorter period of time are dominated by *Eragrostis unamoena*, *Panicum repens*, or *Sorghastrum freesia*. This is followed by a zone dominated by *Imperata cyclindrica*. Moving towards the middle of the island, the vegetation community is dominated by the grass *Miscanthus junceus*. On higher ground on the islands, tall evergreen species such as *Diospyros mespiliformis* are present, with deciduous species such

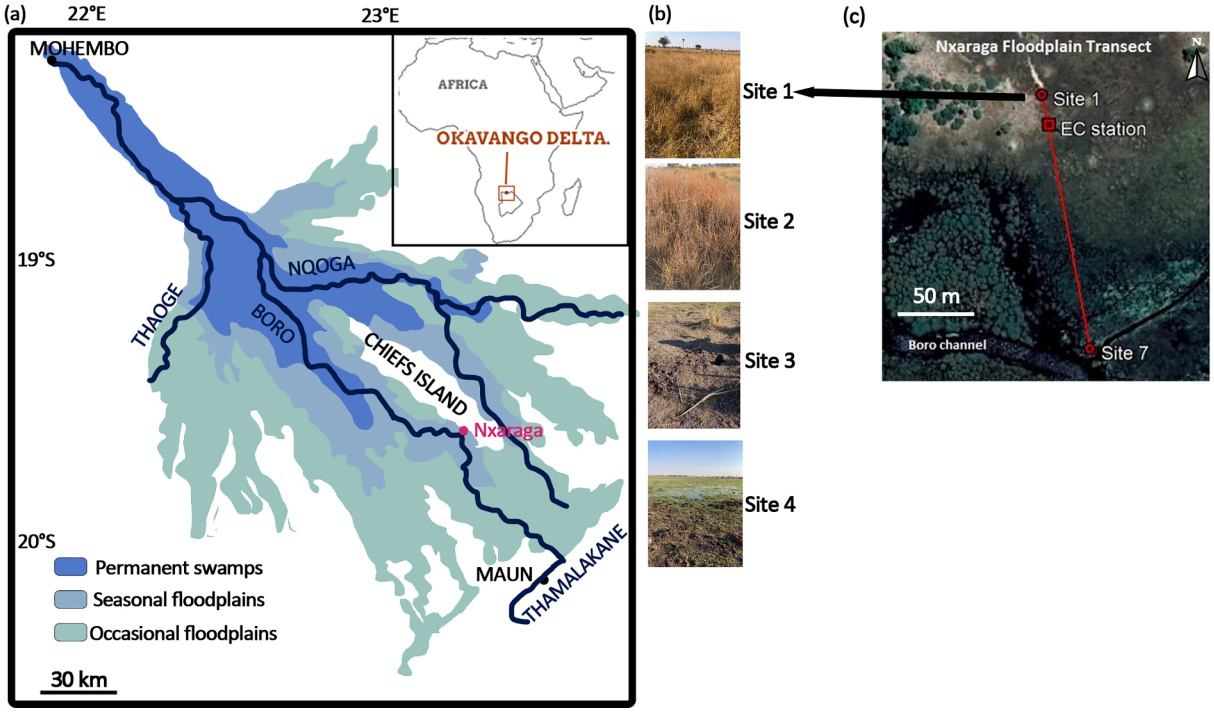

Fig. 1. (a) Map of the Okavango Delta (adapted from Gondwe et al., 2021), (b) pictures of the studied sites (taken in August 2022, site 5–7 were flooded) and (c) soil transect (from Gondwe et al., 2021). EC station is a weather station.

as *Croton megalobotrys* and *Hyphaeane ventrucosa* found further inland (e.g., Ellery et al., 1992; Ellery and McCarthy, 1994; Lubinda, 2012).

The 43 soil samples selected were collected between 2018 and 2021 as part of the NERC funded MOYA Closing the global methane budget project in the Okavango Delta implemented by the UK Centre for Ecology and Hydrology (UKCEH) and the Okavango Research Institute of the University of Botswana. The soil samples were collected from a seasonal floodplain located at Nxaraga area at the southeastern edge of the Chief's Island (Botswana, Fig. 1, Gondwe and Masamba, 2014; Gondwe et al., 2021; Mosepele et al., 2022). As the transect was partly located in the floodplain, and only non-submerged soils were sampled, the selected soils along the transect were spread along 260 m and 7 sites during the low-flood season (February, March). During the high-flood season (August, September) the transect had only 5 sites (~55 m). In August 2022, soil (n = 5) and plant (n = 16) samples along the same transect were collected following the general vegetation zonation described above (see Table 1). C_4 grasses (*Imperata cylindrica, Eragrostis inamoena, Miscanthus junceus*) were dominant around sites 1–3 across the seasons (dry to dominantly dry sites, M. Gondwe, personal communication), whereas for sites 4–7 (seasonally flooded sites), C_4 plants were dominant during the low-flood season while C_3 plants (macrophytes) were present during the high-flood season. This plant succession is typical for the seasonal swamps of the Okavango Delta (Ellery and McCarthy, 1994). Plant carbon metabolism was inferred from previous studies (see references in Table 1) and matched with compound-specific lipid carbon isotopes. When no reference existed, the photosynthetic mechanism (C_3 vs C_4) was inferred only from lipid carbon isotopes obtained during this study.

Plant xylem tissue was sampled in duplicate for trees (*Diospyros lycloides, D. mespiliformis, Hyphaene petersiana, Crotom megabolytr, Kigelia africana, Lonchocarpus capassa*) with a diameter > 10 cm. A core drill sample was extracted (diameter 5 mm, length 400 mm) and the outer layers (epidermis, cortex, bark, phloem) were removed to prevent contamination with phloem sap. For small branches, xylem material was collected as twig pieces, which were debarked using a knife. No xylem tissue was sampled from grasses. Xylem samples were stored in sealed glass vials with rubber/PTFE liners until water extraction. Plant leaves were sampled depending on plant growth form. For grasses, the whole above-ground green plant was sampled in duplicate. For trees and shrubs, fresh leaves were randomly collected at different heights and at the four cardinal points (exposure towards north, east, south, west) and merged into duplicate composite sample representing the entire plant.

Table 1
Plant location and identification, as well as sampling conditions; the plants have been sampled in August 2022 and the sites can be different (except site 1) from the other campaign (Gondwe et al., 2021).

Site	Date	Plant part	Species	Common name	Latitude (°S)	Longitude (°E)	Distance from Site 1 (m)	Temperature (°C)	Residual Humidity (%)	Plant metabolism
Site 1b	Aug-22	Leaf a	*Imperata cylindrica*	Flame grass	−19.5479	23.17905	0	31	22.2	C_4
Site 2b	Aug-22	Leaf a	*Eragrostis inamoena*	Rice grass	−19.5482	23.17918	2	29.4	22.3	C_4
Site 2b	Aug-22	Leaf b	*Imperata cylindrica*	Flame grass	−19.5482	23.17918	2	29.4	22.3	C_4
Site 3b	Aug-22	Leaf a	*Mischamtus junceus*		−19.5485	23.17922	66	30.1	22.2	C_4
Site 4b	Aug-22	Leaf a	*ND*		−19.5488	23.17933	69	31.1	29.3	C_4
Site 5b	Aug-22	Leaf a	*Ludwigia leptocarpa*		−19.5497	23.1795	205	17.1	48.1	C_3
Site 5b	Aug-22	Leaf b	*Vossia cuspidata*	Hippo grass	−19.5497	23.1795	205	17.1	48.1	C_3
Site 5b	Aug-22	Leaf c	*Potamogedon nodosus*		−19.5497	23.1795	205	17.1	48.1	C_3
Site 5b	Aug-22	Leaf d	*Nymphaea nouchali*	Water lily	−19.5497	23.1795	205	17.1	48.1	C_3
Site 5b	Aug-22	Leaf e	*Salvenia minima*	Oxygen weed	−19.5497	23.1795	205	17.1	48.1	C_3
Site 5b	Aug-22	Leaf f	*Neptunia oleracea*		−19.5497	23.1795	205	17.1	48.1	C_3
Site 5b	Aug-22	Leaf g	*Ottelia ulvifolia*		−19.5497	23.1795	205	17.1	48.1	C_3
Site 6b	Aug-22	Leaf a	*Diospyros lycloides*		−19.5471	23.16892	1060	17.1	48.1	C_3
Site 6b	Aug-22	Xylem a	*Diospyros lycloides*		−19.5471	23.16892	1060	17.1	48.1	C_3
Site 6b	Aug-22	Leaf b	*Diospyros mespiliformis*		−19.5471	23.16892	1060	17.1	48.1	C_3
Site 6b	Aug-22	Xylem b	*Diospyros mespiliformis*		−19.5471	23.16892	1060	17.1	48.1	C_3
Site 6b	Aug-22	Leaf c	*Hyphaene petersiania*	Palm tree	−19.5471	23.16892	1060	19.7	38.4	C_3
Site 6b	Aug-22	Xylem c	*Hyphaene petersiania*		−19.5471	23.16892	1060	19.7	38.4	C_3
Site 6b	Aug-22	Leaf d	*Croton megalobotrys*		−19.5471	23.16892	1060	19.7	38.4	C_3
Site 6b	Aug-22	Xylem d	*Croton megalobotrys*		−19.5471	23.16892	1060	19.7	38.4	C_3
Site 7b	Aug-22	Xylem a	*Kigelia africana*	Sausage Tree	−19.5479	23.178	109	21.9	36.7	C_3
Site 7b	Aug-22	Xylem b	*Lonchocarpus capassa*	Rain Tree	−19.5479	23.178	109	21.9	36.7	C_3

ND not determined.

River water was collected in August and September 2022 from the main (Boro) channel close to the Nxaraga transect in duplicate in 1.5 mL vials (without headspace), and stored in the fridge until measurements.

2.2. Bulk soil carbon isotope measurements

For determination of the carbon isotopic compositions ($\delta^{13}C_{bulk}$, the ratio of $^{13}C/^{12}C$ in a sample relative to the standard Vienna PeeDee Belemnite, VPDB) of the soils (n = 43), 15–30 mg of freeze-dried and homogenized soil was fumigated with concentrated hydrochloric acid (HCl 37%) for 72 h at 60 °C to remove inorganic carbon (e.g. calcium carbonates), and subsequently neutralized and dried under a basic atmosphere (pH > 7, NaOH) at 60 °C for another 72 h. Analysis were done with an Elemental Analyzer (EA) coupled to a stable isotope analyzer (EA-IRMS, Elementar vario MICRO cube—Isoprime Precision) (McIntyre et al., 2016). The instrument accuracy during analysis was 0.14‰, the standards used were oxalic acid II (NIST SRM 4990C), phthalic anhydride (Sigma, PN-320064-500g, LN-MKBH1376V), atropine (Säntis, PN-SA990746B, LN-51112), and acetanilide (Merck, PN-100011, LN-K37102211229).

2.3. Plant, river and soil water hydrogen isotope analysis

Leaf, xylem and soil water were extracted from duplicate samples taken during the 2022 campaign. A total of four soils corresponding to sites 1–4 (dry season with flooded channels, August 2022), sixteen leaves and six xylem samples were analysed. The water extraction protocol followed Diao et al. (2022). Briefly, after sampling, the plant parts and soils were kept frozen in gas-tight glass vials (Exetainer; Labco, Lampeter, UK). For the extraction, the vials with samples were attached to a vacuum system. During extraction, the pressure inside the system was maintained below 0.05 mbar using a vacuum pump. The sample tubes containing the soils were additionally blocked by PP fiber filters (Nozzle protection filter, Socorex Isba SA, Ecublens, Switzerland) to avoid soil particles being drawn into the U-tubes with the extracted water or the vacuum pump. The sample tubes were heated in 80 °C water, and the extracted water was condensed and trapped in the collection tubes by liquid nitrogen. The extraction was maintained for 2 h to achieve a complete extraction (West et al., 2006). After the extraction, the vacuum inside the system was released by adding dry nitrogen gas until atmospheric pressure conditions were re-established. Then the collection tubes with frozen water samples were detached from the system and sealed with rubber plugs. The water in the collection tubes was thawed at room temperature. We collected the water droplets and transferred them into 2 mL glass vials with a syringe and 0.45 μm nylon filters to remove potential particles (Infochroma AG, Goldau, Switzerland) using a pipette. The samples were stored at −20 °C before and after the extraction.

The δ^2H (δ^2H, the ratio of $^2H/^1H$ in a sample relative to the Vienna Standard Mean Ocean Water, VSMOW) of the plant and soil water samples were measured with a high temperature conversion elemental analyser coupled to a DeltaPlus XP isotope ratio mass spectrometer (TC/EA-IRMS; Finnigan MAT, Bremen, Germany). Calibration against VSMOW was achieved by analysis of a range of certified water of different isotope ratios, resulting in a precision of analyses of 2‰ for δ^2H.

Hydrogen and oxygen isotope composition of the river water was measured using a PICARRO isotope and gas concentration analyzer (L2130-i). Nitrogen was used as purge gas and the vaporizer temperature was set at 110 °C. There were 12 injections per sample (1.8 μL), six injections were used to flush the vaporizer and measurement cavity of the instrument between samples. The latter six injections were injected as individual pulses for measurement with the latter four used in the data reduction. Isotope compositions were calibrated against reference materials from the International Atomic Energy Agency (IAEA) including SLAP2, GRESP, and VSMOW2 and in-house reference materials, resulting in a precision of analyses of 0.1–2‰. An independent quality control was carried up against reference materials from the United States Geologic Survey (USGS) which were run as quality control.

2.4. Lipid extraction, quantification and compound-specific stable isotope measurements

Freeze-dried soils (2–3 g) and plants (~0.2 g) were extracted with an EDGE system (CEM) as described in Lattaud et al. (2021). Following extraction, the total lipid extract was saponified with 0.5 M potassium hydroxide (KOH) in methanol (MeOH) and the neutral fraction was liquid–liquid extracted three times with hexane. The remaining aqueous solution was acidified (pH ~ 2) and FA were liquid–liquid extracted three times with hexane (Hex): dichloromethane (DCM) (4: 1, *v/v*). The acid fraction was then methylated overnight (12 h, 70 °C) with MeOH: HCl (95: 5, *v/v*) of known isotopic composition, and the resulting FA methyl esters (FAMEs) were liquid–liquid extracted four times with hexane. The neutral fraction was further separated in three fractions on an activated silica oxide column (1% deactivated), the first fraction containing the *n*-alkanes was eluted with hexane.

FAMEs and *n*-alkanes were quantified on a HP 7890A gas chromatograph (GC) equipped with a flame ionization detector (FID), and a VF-1 MS capillary column (30 m × 0.25 mm, 0.25 μm film thickness). The temperature program started with a 1 min hold time at 50 °C, followed by a 10 °C min^{-1} ramp to 320 °C and a 5 min hold time at 320 °C. Peaks were identified against a mix of pure standard compounds based on retention time. To quantify the compounds, a known amount of C_{36} *n*-alkane was run several times as external standard during the same sequence. Paq (used to distinguish between non-emergent aquatic macrophytes and emergent and terrestrial plants) was calculated for FA adapting the equation from Ficken et al. (2000) [Eq. (1)]:

$$Paq = \frac{C_{22} + C_{24}}{C_{22} + C_{24} + C_{28} + C_{30}} \quad (1)$$

Before stable carbon and hydrogen isotope analysis, the FAME fraction was further purified over a silica gel column with Hex: DCM (4: 1, *v/v*) and DCM, with the linear FAMEs ending in the second fraction.

Compound-specific $\delta^{13}C$ analysis of FAMEs were performed within the Climate Geology Group of ETHZ. Samples were run in duplicate and results were calibrated against pulses of CO_2 gas with a known $\delta^{13}C$ value by GC–isotope ratio mass spectrometry (GC–irMS) on a Thermo Trace GC (1310) coupled with a Thermo Delta-V plus system. The GC was equipped with a RTX-200 MS capillary column (60 m × 0.25 mm i.d., 0.25 μm film thickness) and the temperature program was as follows: ramp from 40 °C to 120 °C at 40 °C min^{-1}, followed by a 6 °C min^{-1} ramp to 320 °C and a 12 min hold time at 320 °C. Reproducibility of reference gas peak CO_2 $\delta^{13}C$ values (analysed three times at the beginning and three times end of each sample measurement) did not exceed ±0.09‰. Long-term analytical performance of the instrument is assessed by running *n*-alkane and fatty acid mix standards (A7 and F8 supplied by A. Schimmelmann, Indiana University) and the root mean square errors of $C_{18:0}$, $C_{20:0}$, $C_{22:0}$, $C_{24:0}$, $C_{26:0}$, $C_{30:0}$ did not exceed 0.1‰ throughout sample analysis. Samples (combining three plant or soil replicates) were run in duplicate and differences between repeat measurements of the same analytical sample did not exceed 1‰.

Compound-specific δ^2H analysis of the FA were performed in duplicate on a GC–irMS (Thermo Trace GC Ultra coupled with a Thermo Delta-V plus system). The GC was equipped with a VF-1MS (60 m x 250 μm; 0.25 μm film thickness) column and temperature program was as followed: ramp from 45 °C to 130 °C at 40 °C min^{-1} then to 300 °C at 6 °C min^{-1} and held at 300 °C for 32.5 min. The flow of helium was 1 mL min^{-1}. The H_3^+ factor was determined at the start of each sequence (every other day) and averaged 4.7 ± 0.3 during the course of analyses. To monitor instrument performance a pure C_{27} alkane standard (−173 ± 2‰ supplied by A. Schimmelmann, Indiana University) was measured (average offset during the course of the measurements 1 ± 3‰), and

corrections were made on daily batches for offsets between measured and reported standard values.

The $\delta^{13}C$ and $\delta^{2}H$ values of the FAMEs have been corrected for carbon and hydrogen addition from methylation as follows (Lattaud et al., 2021) [Eq. (2)]:

$$\delta^{i}X_{FAME} = \frac{(nX_{FAME} + nX_{CH3}) \times \delta^{i}X_{FAME}measured - nX_{CH3} \times \delta^{i}X_{CH3}}{nX_{FAME}} \quad (2)$$

With X and ^{i}X either H and ^{2}H or C and ^{13}C.

For $\delta^{2}H$: nH_{FAME} = number of carbon atoms of FAME, $nH_{CH3} = 3$ and $\delta^{2}H_{CH3} = -101 \pm 3‰$. For $\delta^{13}C$: nC_{FAME} = number of carbon atoms of FAME, $nC_{CH3} = 1$ and $\delta^{13}C = -48.1 \pm 0.4‰$.

Fractionation between source water and plant wax lipids (e.g., Sessions et al., 1999; Garcin et al., 2012; Griepentrog et al., 2019) is calculated as follows:

$$\varepsilon_{app} = \left(\frac{\delta^{2}H(fatty\ acids) + 1000}{\delta^{2}H(rain) + 1000} - 1\right) \times 1000 \quad (3)$$

The rain $\delta^{2}H$ from Dincer et al. (1979) was used for this calculation −25.8‰.

$$\varepsilon_{net} = \left(\frac{\delta^{2}H(fatty\ acids) + 1000}{\delta^{2}H(source\ water) + 1000} - 1\right) \times 1000 \quad (4)$$

For plant source water two different water pools were used: (1) river water average in August 4.1 ± 1.7‰ for all aquatic plants, and (2) soil water at each site which varies from −30.6 ± 0.2‰.to −11.8 ± 0.1‰ for C_4 plants. For the trees, both (1) and (2) were tested.

The percentage of C_3 plant cover is calculated following Garcin et al. (2014) to account for the small growth form and lower biomass of C_4 plants:

$$fC_3 = \sin\left(\frac{\pi}{2}\left(\frac{-\delta^{13}C_{soil} + \delta^{13}C_{C3}}{\delta^{13}C_{C3} + \delta^{13}C_{C3}}\right)\right)^{2} \quad (5)$$

3. Results

3.1. Bulk properties

To frame the isotopic values of plant and soil FA, bulk soil $\delta^{13}C$, as well as the $\delta^{2}H$ of river water, soil water and plant water are determined.

Bulk soil $\delta^{13}C$ (n = 43) values vary from −14.2‰ in Site 2 in August 2018 to −24.2‰ in Site 7 in February 2018 (Fig. 2). The average $\delta^{13}C$ value for site 1 is −15.8 ± 0.8‰ (mean ± Std Dev., n = 6), and the average value decreases with distance from site 1 to the main channel, with site 7 on average −22.7 ± 1.1‰ (n = 3) (Supp. Table 1).

Plants Tree leaf water $\delta^{2}H$ values (40.9 ± 8.6‰, n = 6) were high, and indicate a strong enrichment in ^{2}H compared with the xylem water (−21.8 ± 7.1‰, n = 12). For the trees that had both xylem and leaves measured (n = 3, only from site 6b) this enrichment was in the range of 50‰ to 70‰, (Fig. 3C, Supp. Table 4). In addition, the $\delta^{2}H$ values of the tree leaves were high (40.9 ± 8.6‰, 3 trees, each in duplicate) compared with the $\delta^{2}H$ values of the leaves from both aquatic and terrestrial grass plants (1.4 ± 11.5‰, 12 leaves, each in duplicate).

Soils The four soil duplicate samples had a soil water $\delta^{2}H$ range from −11.8 ± 0.1‰ to −30.6 ± 0.2‰ (mean ± Std Dev.) (Fig. 3C, Supplementary Table 4).

River water In contrast to the negative values in soil, river water $\delta^{2}H$ was 4.1 ± 1.7‰ over the two months studied (n = 2, Fig. 3C).

3.2. Fatty acid and n-alkane concentration and distribution

To determine the species-specific distribution and concentration of plant waxes, FA and *n*-alkanes were analysed in plant leaves and in soil samples.

Plants FAME were detected in all plant samples in different concentrations (Fig. 4A) with three species *(C. megalobotrys, V. cuspidata and I. cylindrica*) above 6 μg g^{-1} (sum of all FAME, C_{16}–C_{34}). Longer chain FAME (>C_{28}) were mostly detected in grasses (*I. cylindrica, E. inamoena*, and *M. juncis*) and in one tree (*C. megalobotrys*). On average terrestrial plants (tree and grasses) have 7–20 % C_{28} FAME and 4–9% C_{30} FAME (except *Hyphaena petersiana*, which presented more C_{22} and C_{24} FAME, of up to 67% of all FAME). Both emergent and submerged aquatic plants present <2 μg g^{-1} FAME (Fig. 4A, Supplementary Table 2), submerged plants (*P. nodosus, S. minima, O. ulvifolia*) have shorter chain FAME (C_{16}–C_{22}, 30–67 % of all FAME), whereas emerged plants (i.e., *N. oleacera, V. cuspidata*) have FAME up to C_{32}. Paq varies from 0.12 to 1, with 1 only found in submerged aquatic plants (Supplementary Table 2).

n-alkanes of chain length C_{15}–C_{33} were detected in all samples, but in lower amount than FA (about 10 times lower per gram of plant, Supplementary Table 2). C_{15}–C_{19} *n*-alkanes were observed in only the submerged aquatic *S. minima* (oxygen weed). Some aquatic plants have shorter chain *n*-alkanes such as C_{21}–C_{23} (*S. minima*, *P. nodosus* and *N. nouchali*, 23–33% of all *n*-alkanes), whereas others present a "classic" distribution starting at C_{25}–C_{29}. C_{31}–C_{33} are only detected in trees and grasses. The sum of *n*-alkane concentration varies from 0.03 to 0.98 μg g^{-1}. Paq (the ratio of C_{23} + C_{25} alkanes over the C_{29} + C_{31} alkanes,

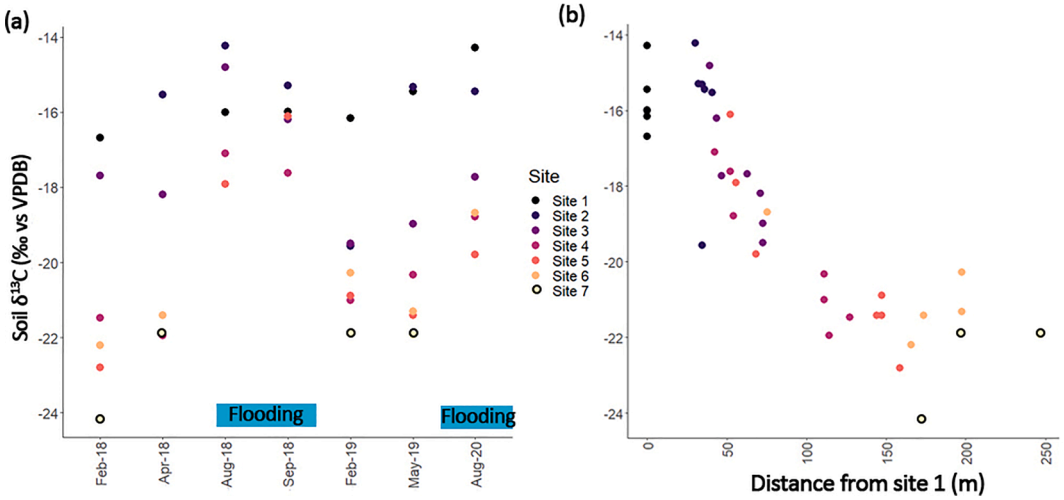

Fig. 2. Bulk soil $\delta^{13}C$ (measurement errors are not visible ± 0.14‰) depending on (a) the month sampled and (b) the distance from site 1. In blue are the periods of flooding of the channels (the soils are always sampled on dry land, not underwater). (For interpretation of the references to colour in this figure legend, the reader is referred to the web version of this article.)

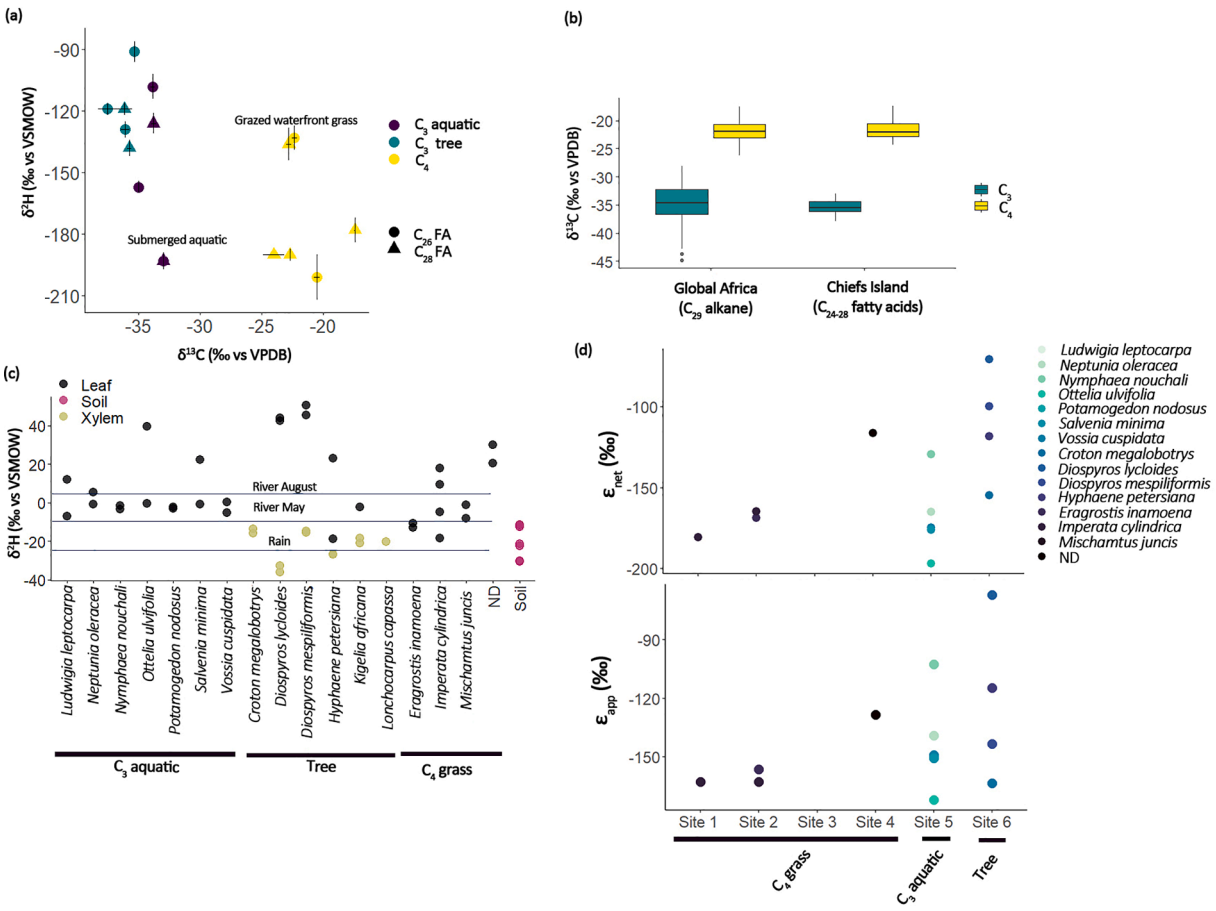

Fig. 3. (a) Compound-specific isotopes (δ^2H and $\delta^{13}C$) of fatty acids of the Okavango Delta plants (this study), and (b) comparison of the $\delta^{13}C$ of the $C_{24\text{-}28}$ fatty acid of the plant of Chiefs Island (this study) with a global dataset of $\delta^{13}C$ of C_{29} alkane in plants in Africa (from Badewien et al., 2015; Bezabih et al., 2011; Ellery et al., 1992; Garcin et al., 2014; Kristen et al., 2010; Magill et al., 2019; Rommerskirchen et al., 2006; Vogts et al., 2009). (c) water δ_2H of the plant tissue (the black lines indicates the values for river water in the Boro Channel from this study and rain water in Maun from Dincer et al., 1979), and (d) net and apparent fractionation for the different plants. Site 6 and 7 are not part of the soil transect and the trees were sampled slightly upstream (Table 1).

Ficken et al., 2000) varies from 0.7 to 1 for the aquatic plants (n = 5), from 0 to 0.49 for the terrestrial plants (n = 9). The C_{25} alkane is present in all plants studied here in varying fractional abundance, and thus is not typical of aquatic plants in the Okavango Delta.

Soils FAME were detected in all soils from C_{16} to C_{32}, the dominant FAME are usually the C_{16} (16 ± 12%) and C_{24} (9 ± 5%) for all soils. Total concentration (sum of C_{16}–C_{32}) varies from 40 to 11800 μg g^{-1}_{OC} (Fig. 4B). *n*-alkanes were detected in the soils (note that for 10 soils chromatography did not allow for *n*-alkanes quantification) from C_{23} to C_{33}, the percentage of C_{31}–C_{33} *n*-alkane (the dominant *n*-alkanes in most soils) varies from 25 to 49%. Paq varied from 0.34 to 1 (Supplementary Table 5).

3.3. Compound-specific carbon and hydrogen isotope ratios of fatty acids

To establish the variation in FA stable isotopic composition for most abundant plant species in the Okavango Delta, and the values of FA that are present in soils their specific $\delta^{13}C$ and δ^2H were measured. Due to the low amount of *n*-alkanes in plants, most plants did not yield any *n*-alkane stable isotope signatures. In addition, some soils (site 1 during February and August 2018) had a complex chromatography that prevented stable isotope analysis. This section and the following discussion will only discuss variation in FA.

Plants FAME $\delta^{13}C$ values are on average −21.6 ± 1.8‰ ($C_{24\text{-}28}$, n = 5) and −22.6 ± 2.6‰ ($C_{16\text{-}22}$, n = 5) for C_4 plants (Fig. 3A). For C_3 plants the values are more ^{13}C-depleted with an average of −35.5 ± 1.5‰ for the $C_{24\text{-}28}$ (n = 9), and −34.9 ± 2.7‰ ($C_{16\text{-}22}$, n = 9). Plant FAME δ^2H values for C_4 plants are on average −172 ± 20‰ ($C_{24\text{-}28}$, n = 4) and −140 ± 30‰ ($C_{24\text{-}28}$, n = 8) for C_3 plants (Fig. 3A). Net fractionation (ε_{net}, FA versus growth water), varies from −70‰ (for *D. lycloides*) to −180‰ (for *I. cylindrica*). The average ε_{net} for the aquatic plants is −168 ± 22‰, for the C_4 grasses −171 ± 7‰, whereas the values for the tree are highly variable (−70 to −151‰) (Fig. 3D). Apparent net fractionation (ε_{app}) is lowest for the trees (−122 ± 36‰), followed by the aquatic plants (−143 ± 23‰) and the C_4 grasses (−161 ± 3‰).

Soils The short-chain FAME ($C_{16\text{-}22}$) C_4-dominated soil have an average of −19.4 ± 2.0‰ and all other sites −23.0 ± 2.3‰ (Fig. 5A). The long-chain FAME ($C_{24\text{-}28}$) average $\delta^{13}C$ value is −20.9 ± 1.2‰ for the C_4-dominated soils (Site 1 and 2, n = 14, Fig. 5B). Their $\delta^{13}C$ shows little seasonal variation (within 1‰). For all other sites (3, 4, 5, 6, 7) the long-chain FAME ($C_{24\text{-}28}$) averaged at −26.5 ± 2.6‰ (n = 29, Fig. 5B). The δ^2H value of the short-chain FA (Fig. 5C) is low for site 1 compared with other sites, with an average of −211 ± 9‰ (n = 6) compared with −188 ± 16‰ (sites 3–7, distance > 40 m, n = 27). Long-chain FAME ($C_{24\text{-}28}$) δ^2H values are −153 ± 13‰ (n = 12) for the C_4-dominated soils (1 and 2) and −158 ± 10‰ (n = 30) for all the other soils (Fig. 5D).

4. Discussion

4.1. Photosynthetic pathways in plants of the Okavango Delta

Plants of the Okavango Delta are well described but a few were not fully characterized with regard to their carbon metabolism (e.g., Ellery et al., 1992, 1993; Martins-Loução et al., 1993; Ellery and McCarthy,

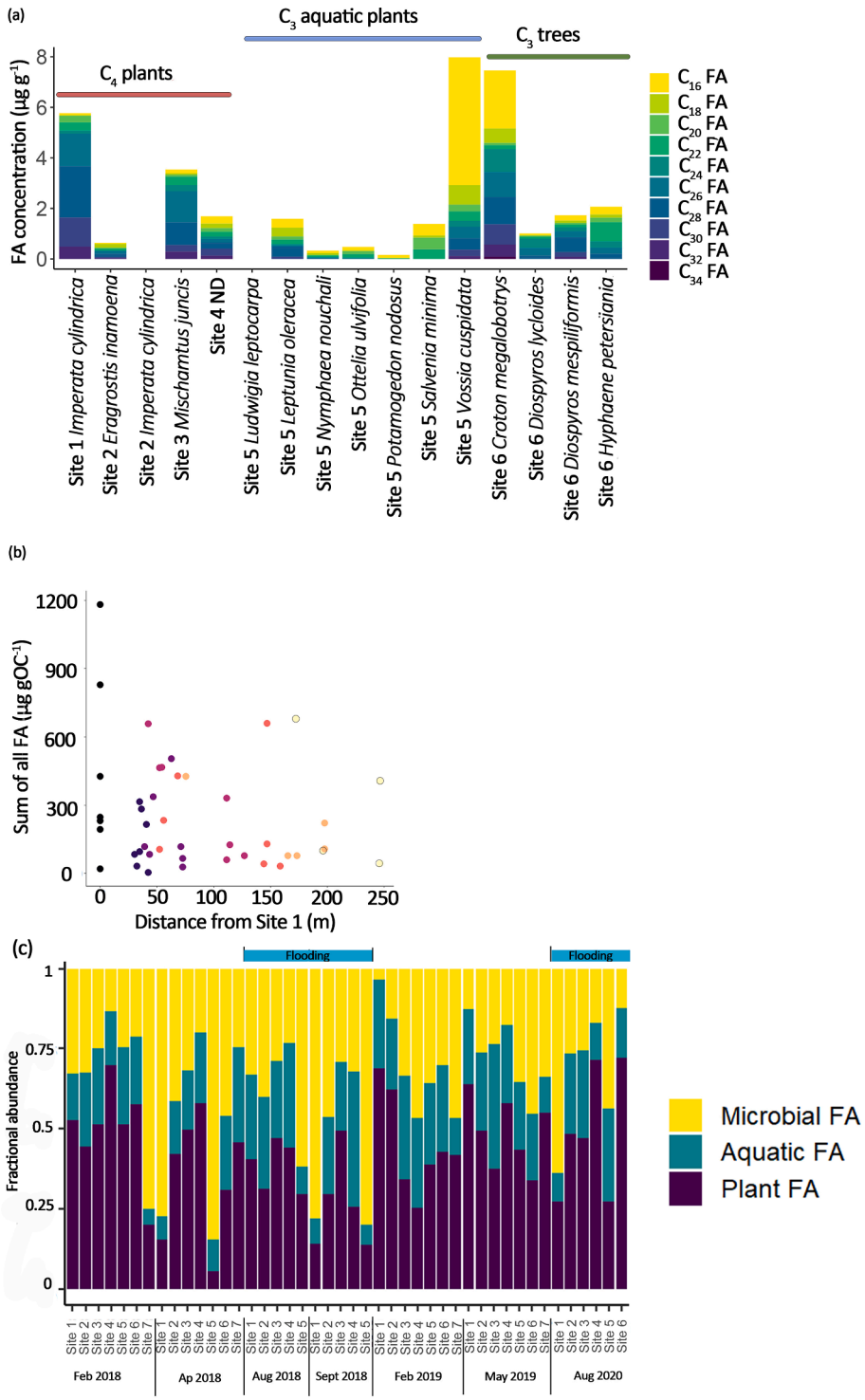

Fig. 4. (a) *n*-fatty acid (FA) concentration in each plants from the transect taken in August 2022, and total FA concentration in the soils (b) depending on the distance from site 1, and (c) FA fractional abundance in the soils depending on the source of FA (microbial, submerged aquatic and higher plants), the period of flooding of the channels is indicated in light blue (the soils sampled are always on land, never underwater). (For interpretation of the references to colour in this figure legend, the reader is referred to the web version of this article.)

1994, 1998; Mantlana et al., 2008; Heath and Heath, 2009; Ritchie, 2012; Pires et al., 2013). Among the 15 species of plants collected in August 2022, all but one were identified down to a species level (site 4 was grazed so short that identification was impossible; Table 1). The photosynthetic pathways of three (*C. megalobotrys, O. ulvifolia, N. nouchali*) studied species have not been previously described. Since this study aimed to define plant stable isotope end-members for C_3 and C_4 plants, their pathway identification is essential. Based on the $\delta^{13}C$ value of the dominant FA (Supplementary Table 3) the photosynthetic pathways (C_3 or C_4) could be determined precisely. *C. megalobotrys* (Euphorbiaceae) likely is a C_3 plant with an average FA $\delta^{13}C$ value of -37.5 ± 0.5 ‰ (average of all chain lengths). *O. ulvifolia* (Hydrocharitaceae) is also a C_3 plant, based on the FA $\delta^{13}C$ value with an average of -32.2 ± 0.9 ‰. Both plants compare well with the average

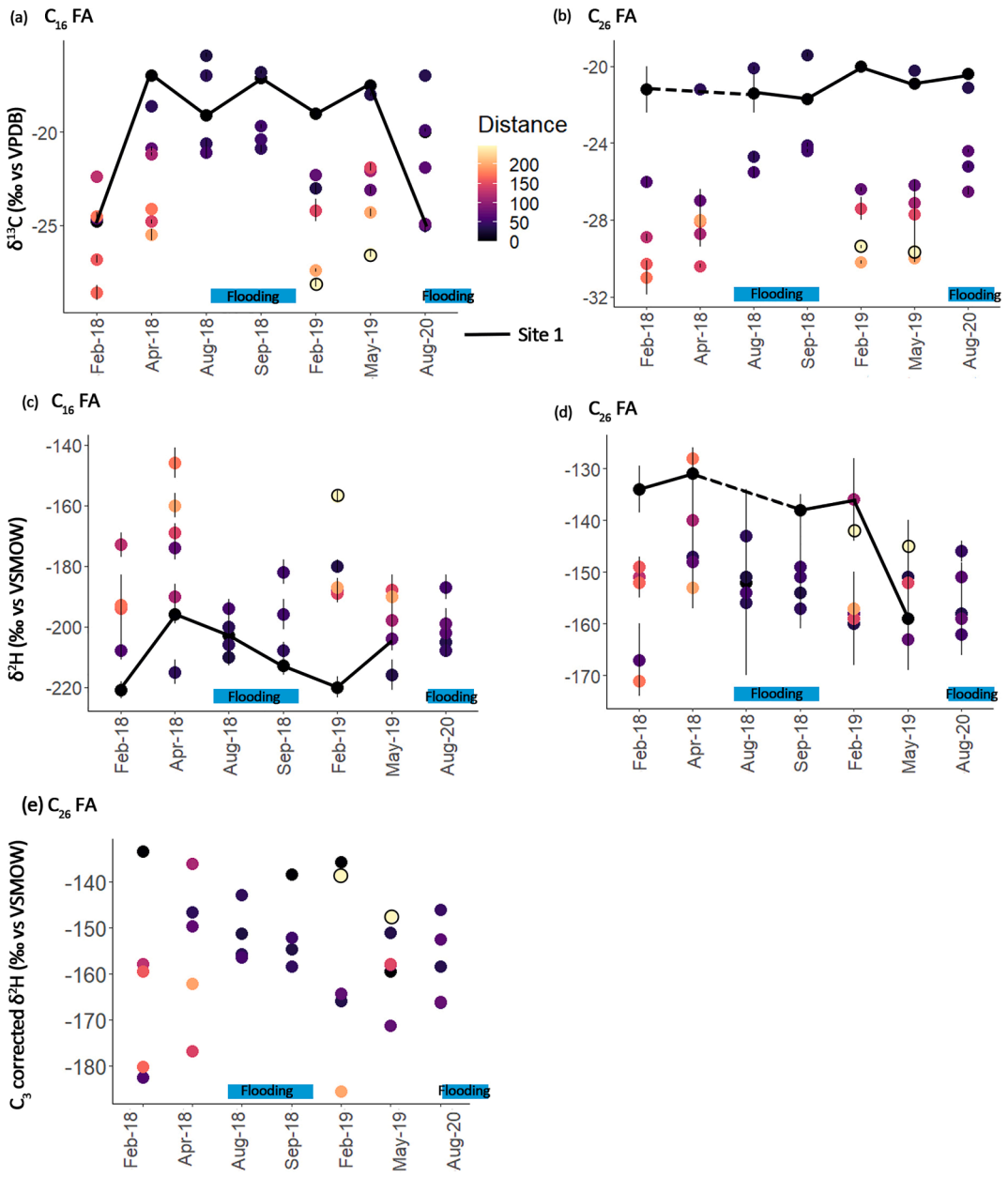

Fig. 5. Compound-specific FA isotope ratios in the soils depending on the distance from site 1: $\delta^{13}C$ of (a) the C_{16} FA, (b) the C_{26} FA, and $\delta^{2}H$ of (c) the C_{16} FA and (d) the C_{26} FA, (e) shows the corrected $\delta^{2}H$ of the C_{26} FA using the modern plant end-member and the fractional abundance of C_3 plants (errors are very large and the values are indicative). The period of flooding of the channels is indicated in light blue (the soils sampled are always on land, never underwater). As only site 1 is always at the same position, only this site is joined by a black line. (For interpretation of the references to colour in this figure legend, the reader is referred to the web version of this article.)

for C_3 plants in Africa of −33 to −35 ‰ for $C_{27\text{-}33}$, *n*-alkanes (Fig. 3B, n = 217, Mooney et al., 1977; Ellery et al., 1992; Ballentine et al., 1998; Rommerskirchen et al., 2006; Vogts et al., 2009; Kristen et al., 2010; Bezabih et al., 2011; Garcin et al., 2014; Badewien et al., 2015; Magill et al., 2019), when accounting for ^{13}C-depleted values of FA of ~1.4 ± 1.1‰ compared with *n*-alkanes which are most often describe in literature (Chikaraishi and Naraoka, 2007). No photosynthetic pathway is described for *N. nouchali* (Nymphaeacea), but other subspecies from the Nymphaeacea family have been reported as C_3 plants (e.g., Ritchie, 2012). The FA of *N. nouchali* has an average $\delta^{13}C$ value of −33.5 ± 0.3‰, agreeing with a C_3 pathway. The unidentified plants from Site 4 is likely a C_4 plant, based on $\delta^{13}C$ values of the FA of −21.9 ± 0.6‰, within the range of C_4 plant in Africa −21.0 to −22.1‰ for $C_{27\text{-}33}$-alkanes (Fig. 3B, n = 117, Mooney et al., 1977; Ellery et al., 1992; Ballentine et al., 1998; Rommerskirchen et al., 2006; Vogts et al., 2009; Kristen et al., 2010; Bezabih et al., 2011; Garcin et al., 2014; Badewien et al., 2015; Magill et al., 2019) accounting for a similar fractionation during FA synthesis (1.4 ± 1.1‰) (Chikaraishi and Naraoka, 2007). Hence, we can define C_3 and C_4 end-members for this transect (there is no differentiation of the C_3 macrophyte and the C_3 trees), with an average C_4 plant $\delta^{13}C$ value of −21.4 ± 2.0‰ and $\delta^{2}H$ value of −173 ± 21‰ and for C_3 plants an average $\delta^{13}C$ value of −35.5 ± 1.5‰ and $\delta^{2}H$ value of −144 ± 31‰. In summary, and in agreement with previous work in Africa, C_3 and C_4 plants along the Nxaraga transect in Chief's Island are distinct in term of FA $\delta^{13}C$ composition (Fig. 3B).

4.2. Plant water source and biosynthetic hydrogen fractionation

The plant source water in the Okavango Delta could be rain, river water/groundwater (Ramberg et al., 2006; Jolivet et al., 2023), and soil water (with a variable impact of evaporation). Rain water δ^2H values recorded in Maun by Dincer et al. (1979) (taken in April and June, n = 2) are on average −25.8‰, while river water in the Boro channel was +4.1‰ in August/September 2022, but was −13 to −19.4‰ in May 1975 (peak flooding, Dincer et al., 1979), indicating a large effect of evaporation between the start of the flooding (in May/June) and August (Fig. 3C). However, there is a lack of water isotope data from both river water and precipitation, especially covering seasonality and intra-annual variability, which hinder this interpretation. Both rain and river water (during the flooding season) are more ^2H-depleted than soil water (−11.9‰). The likely origin of soil water is river water, as the small amount of rain is almost immediately evaporated (Andersson et al., 2003; Ramberg et al., 2006). In addition, groundwater from boreholes and piezometers dug in the delta have similar δ^2H value to the river water in May (Dincer et al., 1979; Jolivet et al., 2023). In our study site, rain, soil and river water δ^2H values are sufficiently different to allow for the determination of the source of plant water by looking at the non-fractionated plant xylem δ^2H values. However, more recent rain water isotope signature and a seasonal river water isotope signature would help with the validation of these results.

Out of 6 trees, four trees have xylem water that is slightly ^2H-depleted compared to river water (−17.2 ± 2.3‰, Fig. 3C), indicating potential river water incorporation (in agreement with Ehleringer and Dawson, 1992). The depth of the water table (river-water fed) is around 150 cm deep at this location, which is relatively shallow, hence all trees should be able to access this water (Bauer-Gottwein et al., 2007). In comparison, xylem water for two trees are ^2H-depleted (−30.8 ± 3.8‰, Fig. 3C) compared to rain water which indicate that they do not source their water directly from the river. This implies another water source, different from those mentioned above and less likely to reflect evaporated water. Jolivet et al. (2023) mentioned the presence of a deeper aquifer, independent from the upper river-fed one which could be their water source. The xylem isotope ratios are independent from the growth form of the tree, e.g. *K. africana* is a deep-rooted tall tree while *D. lycloides* is a shrub-like tree and they have very similar xylem water δ^2H (Supplementary Table 4). Hence variation in xylem water in this small sample set is mainly driven by source water, similarly to what Griepentrog et al. (2019) observed.

Leaf water is more ^2H-enriched than the corresponding xylem water (by +66 ± 12‰ for *D. lycloides*, *D. mespiliformis*, and *H. petersiania*), which was previously reported and is caused by transpiration (Cernusak et al., 2016). The offset between xylem and leaf water is larger in the Okavango Delta (50–70‰) than in the Amazon (15 ± 22‰, Feakins et al., 2016), likely due to enhanced transpiration (Sutcliff and Parks, 1989), but is similar to those observed in arid environments such as California (74‰, Feakins and Sessions, 2010). Net fractionation (ε_{net}, between source water – either river or soil – and lipids, following the source water indicated by the xylem) for these C_3 trees varies from −95 to −189‰ (Fig. 3D). Apparent fractionation (ε_{app}, between rain water and lipid) varies from −67 to −164‰, which is similar to ε_{app} usually reported for *n*-alkanes of C_3 plants from tropical and temperate environments (−117 ± 27‰, Sauer et al., 2001; Sachse et al., 2004; Garcin et al., 2012; Schwab et al., 2015; Feakins et al., 2016; Daniels et al., 2017), arid environments (−90‰, Feakins and Sessions, 2010) and ε_{app} of FA from a temperate area (−97‰, Freimuth et al., 2017, 2020). In summary, these trees show a large variation in ε_{app}, mainly due to biosynthetic fractionation and not variation in source water, which might be problematic for interpreting past isotopic signatures. This might be resolved by looking at the relative contribution of tree FA to soil FA and correcting soil FA δ^2H for tree input.

The grasses from sites 1 to 3 are all C_4, and likely take up water directly from surface soil (due to their shallow roots, Schwab et al., 2015) and the ^2H-enrichment of leaves compared with surface soil water is minimum at these sites (13 ± 14‰). One characteristic of C_4 photosynthesis is the reduction of photorespiration by concentrating CO_2 around the RuBisCO enzyme, which allows high rates of photosynthesis at higher temperatures, hence rendering C_4 plants more competitive in arid environments because of reduced water losses (Osborne and Sack, 2012). The C_4 grasses net fractionation (ε_{net}, C_{28} FA versus soil water) is on average −171 ± 7‰ (n = 3, Fig. 3D) which is higher than for *n*-alkanes of C_4 plants (e.g., −132 ± 12‰ for Chikaraishi and Naraoka, 2003 and −90 ± 21‰ for Feakins and Session, 2010). However, there likely is a −25‰ difference between FA and *n*-alkanes, making these ε_{net} similar to other reported C_4 plants (e.g., Sachs et al., 2012). The overgrazed C_4 plant from site 4 has a very ^2H-enriched leaf tissue, indicating major transpiration, while its FA δ^2H value is more similar to those of the aquatic plant, indicating that it might use a mixed water source, i.e. river water (due to proximity) and surface soils (Fig. 3A).

For the C_3 aquatic plants, their source water is likely the river (δ^2H = 4.1 ± 1.7‰), and the fractionation between leaves and river is very small (for the leaves δ^2H = −1 ± 8‰, n = 7), as expected as these macrophytes do not transpire (Sessions et al., 1999; Chikaraishi and Naraoka, 2003; Huang et al., 2004). Their ε_{net} (with the river water as source water) is on average −168 ± 22‰, which is not significantly larger than the C_4 grasses (Fig. 3D). Net fractionation (ε_{net}) from macrophyte was previously reported to be −136 ± 9‰ for *n*-alkanes (Chikaraishi & Naraoka, 2003, 2007). The FA from the aquatic plants are enriched in ^2H and depleted in ^{13}C compared with the C_4 grasses except for the submerged *O. ulvifolia*, which shows low δ^2H values for the C_{26} and C_{28} FA (Fig. 3A).

In summary, the FA δ^2H and $\delta^{13}C$ values of the plants allow for the differentiation of C_3 tree and C_4 grasses. However, care should be given when interpreting hydrogen isotope signatures from extensively grazed grasses closer to the river channel. The δ^2H values of FA from C_3 aquatic plants are similar to those of trees but they have very low amount of FA per plant (except for *V. cuspidata*; Fig. 4A), hence it is unclear if their signal will be preserved over time.

4.3. Preservation of a hydrological signal in soils

To assess how the vegetation and hydrological signal are preserved in the soils, the FA signature of soils and plants are compared. As the plants collected along the transect showed clear end members in terms of $\delta^{13}C$ and δ^2H values (Fig. 3A), tacking the two different pools of plant material into the soils is possible. In addition, rainwater and river water δ^2H values are distinct enough to be able to track hydrological changes (especially which water is primarily used by plants) into the soils. It is to be noted that 2019 was the driest year since 1934 with less than 3500 km^2 of the delta inundated against ~7000 km^2 of average inundation extent between 1985 and 2018 (Inman and Lyons, 2020; Lourenco and Woodborne, 2023).

4.3.1. Origin of FA in soils

Bulk organic stable carbon isotopes ($\delta^{13}C$) indicate a strong temporal (Fig. 2A) and spatial (Fig. 2B) variability of organic matter input into the soils (especially for sites 4–6). Sites 1 and 7 have relatively stable $\delta^{13}C$ values over time (−15.8 ± 0.8‰ and −22.7 ± 1.1‰, respectively), site 5 varies from −16.1‰ (in September) to −22.8‰ (in February) (Fig. 2). As sites 4–6 were not always located at the same distance from site 1 (Gondwe et al., 2019; Fig. 2A), and vegetation changes along this gradient, the sites were under more C_4 vegetation (closer to site 1) and C_3 vegetation (further away from site 1) during the dry-flooding (i.e., August) and rainy-dry channel (February) seasons, respectively. However, to confirm that a change in C_3–C_4 vegetation causes the bulk $\delta^{13}C$ signal, the compound-specific signal needs to match this interpretation. Looking at the long-chain FA $\delta^{13}C$ values in soils, there is always an offset between $\delta^{13}C$ values of the bulk soils and $\delta^{13}C$ values of the FA, varying from −4.7 to −7.5‰, and no significant difference is observed

for C_4-soils versus C_3-soils (offset of −5.3 ± 1.1‰ and −6.8 ± 1.9‰, respectively, Supplementary Fig. 1). This offset likely comes from photochemical alteration and microbial respiration in the soils (e.g., Vähätalo and Wetzel, 2008; Werth and Kuzyakov, 2010). Hence, the FA $\delta^{13}C$ value seems preferable, i.e., more stable, to trace plant organic matter input in soils rather than the $\delta^{13}C$ value of bulk organic matter, which is consistent with previous studies (e.g. Reiffarth et al., 2016).

In terms of source, long chains ($C_n > C_{20}$) are typical of higher plants (e.g., Eglinton and Eglinton, 2008), whereas short chain FA ($C_{16\text{-}18}$) originate dominantly from secondary microbial production (Naafs et al., 2004; Matsumoto et al., 2007) and, in this region, large herbivore fecal matter, especially during the dry season (Reiffarth et al., 2016). Short-chain FA increase in soils dilutes the fractional abundance of plant-derived long chain FA ($C_n > C_{24}$). In addition, mid-chain FA (C_{20}–C_{24}) can be derived from aquatic plants (Ficken et al., 2000). Paq is a useful proxy to track aquatic plant input, and it shows that all submerged plants have a ratio equal to 1 (Supp. Table 2) while the rest (included emerged aquatic plants) have very variable Paq (0.12–0.83; Supp. Table 2). In summary, C_{26}–C_{30} FA will be used to track terrestrial plant input while $C_{16\text{-}18}$ FA will be used to track bacterial input.

The $\delta^{13}C$ value of the $C_{26\text{-}28}$ FA at site 1 and 2 is constant (−21.8 ± 1.8‰, Fig. 5C), likely representing an input of uniquely C_4 plants, with the $\delta^{13}C$ value of the $C_{26\text{-}28}$ FA close to the C_4 end member of the modern plants −21.4 ± 2‰ (Fig. 3A). The small variability in bulk $\delta^{13}C$ values of site 1 and 2 (Fig. 2A, B), is thus proposed to be derived from variability in the $\delta^{13}C$ values of the plant waxes. On the other hand, for site 3–7 there is always a significant increase in $\delta^{13}C$ values from the wet (dry channel) season (February) to the flooding season (August), which is attributed to a change in the location and relative dominance of C_3 trees and C_4 grasses. For example, for the C_{26} FA a change from −31‰ to −24‰ is observed between February 2018 and August 2018. Using the defined end-members (i.e. −21.4 ± 2.0‰ for C_4 grasses and −35.5 ± 1.5‰ for C_3 plants), the proportion of C_4 plants can be calculated (using either a linear or sinusoidal equation, with the latter better representing the smaller life form of C_4 plants compared with C_3 plants (Magill et al., 2019). Across this strong gradient in C_3–C_4 vegetation, the reconstructed proportion of C_4 plants varies from 20 to 90% in sites 4–7 (Fig. 6) and explains the variation in bulk $\delta^{13}C$ values at these sites. To constrain the variability of $\delta^{13}C$ values in the microbially-derived organic matter, we evaluate the $\delta^{13}C$ values of the C_{16} short chain microbial FA. In contrast to the long-chain FA, its $\delta^{13}C$ value is always lower during the rainy season (February 2018 and 2019), and gets higher towards the dry season (August 2018 and 2020) (Fig. 5A). During the rainy season, there is likely a change in the microbial community, changing the type of fractionation occurring during the biosynthesis of the C_{16} FA.

In summary, the bulk organic matter $\delta^{13}C$ values in soils is dominantly explained by the plant-derived organic matter. Sites 1 and 2 have constant C_4 plant inputs (FA ≥ C_{22}) whereas sites 3–7 have seasonal inputs of C_3 and C_4 plants (FA ≥ C_{22}). The impact of microbial-derived organic matter is observed in the composition of soil FA (Fig. 5A), but there is no clear impact of microbial activity on the bulk soil $\delta^{13}C$ values, except for some season (February) and some sites (5–7). As C_3 and C_4 plants fractionate hydrogen differently (Chikaraishi and Naraoka, 2003; Sachse et al., 2012; Chikaraishi et al., 2004), it is important to know their proportion, to allow correction of δ^2H values for the effects of changes in vegetation.

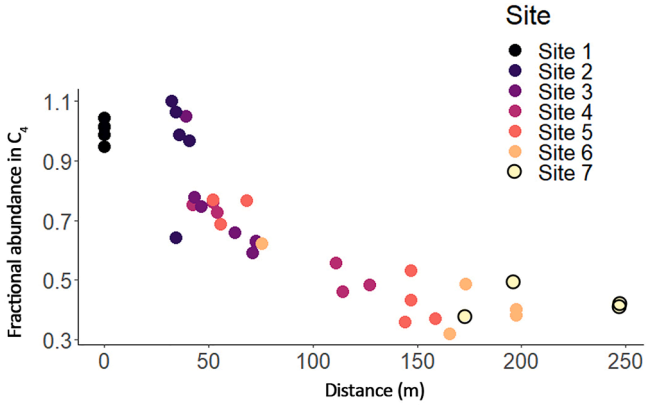

Fig. 6. Fractional abundance of C_4 plants based on FA $\delta^{13}C$ values in the soils, calculated following Garcin et al. (2014).

4.3.2. *δ^2H signal of FA in soils*

The hydrogen isotope values of plant waxes in the Okavango delta are expected to reflect both the change in source water and plant metabolism (Fig. 3). Here, C_3 plants access river water, while C_4 plants access surface soil water that can be strongly ^2H-enriched. However, at Site 1, with a permanent C_4 vegetation (Fig. 6) and disconnected from the (deep) river aquifer, the δ^2H values of the C_{26} FA vary, following a pattern with ^2H-enriched signature during the rainy season (~−140 ‰, February 2018, 2019, April 2018) and ^2H-depleted signature during the dry season (~−160 ‰, August 2018, 2020-September 2018; Fig. 5D). It is important to note that the driest soils are present in the rainy summer season. The impact of evaporation on soil ^2H signal can be seen in the offset between February and August values. In addition, the δ^2H signal of C_{26} FA in site 1 during the dry season is high compared to the C_{26} FA δ^2H values measured on the plant leaves of the same site (−180‰, Fig. 3C), potentially indicating interannual difference in isotopic composition of the water. In addition to changes in soil water evaporation, sites 5–7 (>50 m from site 1) are strongly impacted by change in higher plant input (C_3 versus C_4), and long-chain FA δ^2H values need to be corrected for C_3 plant input using modern plant end-member (δ^2H_{C3} = −144 ± 21‰, Fig. 3A). The estimated amount of C_3 plants is based on the calculation defined by Garcin et al. (2014), which assumes a non-linear evolution of the amount of C_4 plants with its cover extension. It yields more lower δ^2H values for the C_{26} FA (between 30 and 2‰ difference, Fig. 5E). After performing this correction on the C_{26} FA, February (wet season) is the most ^2H-depleted month at sites 5–7, with δ^2H values from sites further away from site 1 also lower (Fig. 5E). The former is an effect of temperature and evaporation whereas the latter could indicate the increased input of submerged macrophytes as these plants have a relatively high ^2H-depletion in their FA (Fig. 3A). However, it is to be noted that the amount of FA present in these plants is very limited, hence, a large amount of these plants is needed to overprint the soil signal. In conclusion, when the source of plant material (C_3 trees vs C_4 grasses) is stable or constrained, δ^2H values of FA reflect evaporation of source water. However, there is a potential for an effect from aquatic submerged plants when they are present in large quantities.

In principle independent from the long-chain FA, and instead governed by the metabolism of distinct bacteria (Heinzelmann et al., 2015; Wijker et al., 2019), the δ^2H of short-chain FA also shows variation in soils (Fig. 5A, C). In general, there is a ^{13}C-depleted and ^2H-enriched C_{16} FA in site 6 and 7, whereas, in site 1 and 2 there is a ^{13}C-enriched and ^2H-depleted C_{16} FA. This could be indicative of the use by microbe of ^{13}C-depleted carbon source and ^2H-depleted water. This reflects the carbon source (C_3 plant-derived organic matter) and soil water source available to the microbes in these soils. The isotopic composition of short-chain FA, such as the C_{16}, can give valuable information about bacterial activity related to the type of plants present and humidity.

5. Conclusion

In this study, modern plants and soils along a seasonally flooded river to island transect in the Okavango Delta showed a typical C_4–C_3 plant zonation as the moisture availability increases. Plant photosynthetic pathways determined using $\delta^{13}C$ of plant-wax-derived FA agree with previous studies, and are the main determinant of soil $\delta^{13}C$ values of bulk organic matter. Apparent and net hydrogen fractionation of the

modern C_3 plants show a strong variation, whereas C_4 plants are more homogenous. Tree xylem water isotope values show that they are not sourcing their growth water from surface soil but use either riverine or deep aquifer water. The soil FA represent an input of C_4 grasses (in the perennially dry site) or a C_3 and C_4 grasses mix in the seasonally flooded sites. The FA δ^2H values of C_4 grasses at the site, which is not impacted by flooding, track the seasonal variation in hydrology in the delta with ^2H-enriched values in the wet season reflecting less evaporation in the soil water. In the other sites, there is a likely influence of submerged macrophytes, although they produce small amounts of FA, as the δ^2H value becomes lower near the river channel. The hydrological source water signal (plant water source) is consistently preserved in the corresponding soil long-chain FA δ^2H values, reflecting both the type of plants and their water usage. To avoid overprint by submerged macrophyte input and the preservation of a hydrological signal it is best to use soils coming from near the channel but in never flooded area.

CRediT authorship contribution statement

Julie Lattaud: Writing – original draft, Visualization, Resources, Project administration, Methodology, Conceptualization. **Mangaliso J. Gondwe:** Writing – review & editing, Resources, Methodology. **Matthias Saurer:** Writing – review & editing, Methodology. **Carole Helfter:** Writing – review & editing, Resources, Funding acquisition. **Cindy De Jonge:** Writing – review & editing, Project administration, Funding acquisition.

Declaration of competing interest

The authors declare that they have no known competing financial interests or personal relationships that could have appeared to influence the work reported in this paper.

Data availability

All data used in this manuscript are in the supplementary information or table within the manuscript.

Acknowledgments

We thank two anonymous reviewer and the editor N. Pedentchouk for their time and comments, that improved the manuscript. H. Lattaud, field assistant, T. Kemosedile and E. Kambato, field technicians of the Okavango Research Institute that assisted during the campaign and plant identification are thanked. In addition, plant identification was possible thanks to the members of the Okavango Research Institute. We thank several people that allowed field sampling and measurements: A. Verstege from WSL, Birmensdorf provided the tree corers, extractions of the plants were done by N. Santoro, and compound-specific carbon isotopes were measured at the Climate Geology Group of the ETH Zurich with the help of R. Wijker. In addition, elemental soil analyses were performed in conjunction with the Laboratory for Ion Beam Facility in ETH Zurich with the help of N. Haghipour. Plant water isotopes have been analysed at WSL Birmensdorf with the help of M. Oettli. Water isotopes have been measured with the help of T. Blattman at the Geological Institute of ETHZ. This work was supported by an ETH commission grant (OKAPI, ETH 2020-1) to C. De Jonge. This research has been carried under the Research permit ENT/8/36/4 LIII(44) from the Ministry of environment, natural resources, conservation and tourism of Botswana.

Appendix A. Supplementary material

Supplementary data to this article can be found online at https://doi.org/10.1016/j.orggeochem.2024.104832.

References

Andersson, L., Gumbricht, T., Hughes, D., Kniveton, T., Ringrose, S., Savenije, H., Todd, M., Wilk, J., Wolski, P., 2003. Water flow dynamics in the Okavango River Basin and Delta—a prerequisite for the ecosystems of the Delta. Physics and Chemistry of the Earth 28, 1165–1172. https://doi.org/10.1016/j.pce.2003.09.002.

Badewien, T., Vogts, A., Rullkötter, J., 2015. N-Alkane distribution and carbon stable isotope composition in leaf waxes of C_3 and C_4 plants from Angola. Organic Geochemistry 89–90, 71–79. https://doi.org/10.1016/j.orggeochem.2015.09.002.

Ballentine, D.C., Macko, S.A., Turekian, V.C., 1998. Variability of stable carbon isotopic compositions in individual fatty acids from combustion of C_4 and C_3 plants: implications for biomass burning. Chemical Geology 152, 151–161. https://doi.org/10.1016/S0009-2541(98)00103-X.

Bauer-Gottwein, P., Langer, T., Prommer, H., Wolski, P., Kinzelbach, W., 2007. Okavango Delta Islands: interaction between density-driven flow and geochemical reactions under evapo-concentration. Journal of Hydrology 335, 389–405. https://doi.org/10.1016/j.jhydrol.2006.12.010.

Bezabih, M., Pellikaan, W.F., Tolera, A., Hendriks, W.H., 2011. Evaluation of n-alkanes and their carbon isotope enrichments ($\delta^{13}C$) as diet composition markers. Animal 5, 57–66. https://doi.org/10.1017/S1751731110001515.

Burrough, S.L., Thomas, D.S.G., Shaw, P.A., Bailey, R.M., 2007. Multiphase quaternary highstands at Lake Ngami, Kalahari, northern Botswana. Palaeogeography, Palaeoclimatology, Palaeoecology 253, 280–299. https://doi.org/10.1016/j.palaeo.2007.06.010.

Burrough, S.L., Thomas, D.S., 2013. Central southern Africa at the time of the African Humid Period: a new analysis of Holocene palaeoenvironmental and palaeoclimate data. Quaternary Science Reviews 80, 29–46. https://doi.org/10.1016/j.quascirev.2013.08.001.

Cernusak, L.A., Barbour, M.M., Arndt, S.K., Cheesman, A.W., English, N.B., Feild, T.S., Farquhar, G.D., 2016. Stable isotopes in leaf water of terrestrial plants. Plant, Cell & Environment 39 (5), 1087–1102. https://doi.org/10.1111/pce.12703.

Chevalier, M., Chase, B.M., Quick, L.J., Dupont, L.M., Johnson, T.C., 2021. Temperature change in subtropical southeastern Africa during the past 790,000 yr. Geology 49, 71–75. https://doi.org/10.1130/G47841.1.

Chikaraishi, Y., Naraoka, H., Poulson, S.R., 2004. Carbon and hydrogen isotopic fractionation during lipid biosynthesis in a higher plant (Cryptomeria japonica). Phytochemistry 65 (3), 323–330. https://doi.org/10.1016/j.phytochem.2003.12.003.

Chikaraishi, Y., Naraoka, H., 2003. Compound-specific δD-$\delta^{13}C$ analyses of n-alkanes extracted from terrestrial and aquatic plants. Phytochemistry 63, 361–371. https://doi.org/10.1016/S0031-9422(02)00749-5.

Chikaraishi, Y., Naraoka, H., 2007. $\Delta^{13}C$ and δD relationships among three n-alkyl compound classes (n-alkanoic acid, n-alkane and n-alkanol) of terrestrial higher plants. Organic Geochemistry 38, 198–215. https://doi.org/10.1016/j.orggeochem.2006.10.003.

Daniels, W.C., Russell, J.M., Giblin, A.E., Welker, J.M., Klein, E.S., Huang, Y., 2017. Hydrogen isotope fractionation in leaf waxes in the Alaskan Arctic tundra. Geochimica et Cosmochimica Acta 213, 216–236. https://doi.org/10.1016/j.gca.2017.06.028.

Dawson, T.E., Ehleringer, J.R., 1991. Streamside trees that do not use stream water. Nature 350, 6316. https://doi.org/10.1038/350335a0.

Diao, H., Schuler, P., Goldsmith, G.R., Siegwolf, R.T.W., Saurer, M., Lehmann, M.M., 2022. Technical note: On uncertainties in plant water isotopic composition following extraction by cryogenic vacuum distillation. Hydrology and Earth System Sciences 26, 5835–5847. https://doi.org/10.5194/hess-26-5835-2022.

Dincer, T., Hutton, L.G., Kupee, B.B.J., 1979. Study, using Stable Isotopes, of Flow Distribution, Surface-Groundwater Relations and Evapotranspiration in the Okavango Swamp. IAEA, Botswana.

Douglas, P.M.J., Pagani, M., Brenner, M., Hodell, D.A., Curtis, J.H., 2012. Aridity and vegetation composition are important determinants of leaf-wax δD values in southeastern Mexico and Central America. Geochimica et Cosmochimica Acta 97, 24–45. https://doi.org/10.1016/j.gca.2012.09.005.

Eglinton, T.I., Eglinton, G., 2008. Molecular proxies for paleoclimatology. Earth and Planetary Science Letters 275, 1–16. https://doi.org/10.1016/j.epsl.2008.07.012.

Ehleringer, J.R., Dawson, T.E., 1992. Water uptake by plants: perspectives from stable isotope composition. Plant, Cell & Environment 15, 1073–1082. https://doi.org/10.1111/j.1365-3040.1992.tb01657.x.

Ellery, K., Ellery, W.N., Verhagen, B.T., 1992. The distribution of C_3 and C_4 plants in a successional sequence in the Okavango Delta. South African Journal of Botany 58, 400–402. https://doi.org/10.1016/S0254-6299(16)30829-8.

Ellery, W.N., Ellery, K., McCarthy, T.S., 1993. Plant distribution in islands of the Okavango Delta, Botswana: determinants and feedback interactions. African Journal of Ecology 31, 118–134. https://doi.org/10.1111/j.1365-2028.1993.tb00526.x.

Ellery, W.N., McCarthy, T.S., 1994. Principles for the sustainable utilization of the Okavango Delta ecosystem, Botswana. Biological Conservation 70, 159–168. 10.1016/0006-3207(94)90284-4.

Feakins, S.J., Bentley, L.P., Salinas, N., Shenkin, A., Blonder, B., Goldsmith, G.R., Ponton, C., Arvin, L.J., Wu, M.S., Peters, T., West, A.J., Martin, R.E., Enquist, B.J., Asner, G.P., Malhi, Y., 2016. Plant leaf wax biomarkers capture gradients in hydrogen isotopes of precipitation from the Andes and Amazon. Geochimica et Cosmochimica Acta 182, 155–172. https://doi.org/10.1016/j.gca.2016.03.018.

Feakins, S.J., Sessions, A.L., 2010. Controls on the D/H ratios of plant leaf waxes in an arid ecosystem. Geochimica et Cosmochimica Acta 74, 2128–2141. https://doi.org/10.1016/j.gca.2010.01.016.

Ficken, K.J., Li, B., Swain, D.L., Eglinton, G., 2000. An n-alkane proxy for the sedimentary input of submerged/floating freshwater aquatic macrophytes. Organic Geochemistry 31, 745–749. https://doi.org/10.1016/s0146-6380(00)00081-4.

Freimuth, E.J., Diefendorf, A.F., Lowell, T.V., 2017. Hydrogen isotopes of n-alkanes and n-alkanoic acids as tracers of precipitation in a temperate forest and implications for paleorecords. Geochimica et Cosmochimica Acta 206, 166–183. https://doi.org/10.1016/j.gca.2017.02.027.

Freimuth, E.J., Diefendorf, A.F., Lowell, T.V., Bates, B.R., Schartman, A., Bird, B.W., Landis, J.D., Stewart, A.K., 2020. Contrasting sensitivity of lake sediment n-alkanoic acids and n-alkanes to basin-scale vegetation and regional-scale precipitation δ^2H in the Adirondack Mountains, NY (USA). Geochimica et Cosmochimica Acta 268, 22–41. https://doi.org/10.1016/j.gca.2019.08.026.

Gao, L., Edwards, E.J., Zeng, Y., Huang, Y., 2014. Major evolutionary trends in hydrogen isotope fractionation of vascular plant leaf waxes. PLoS One1 9, e112610. https://doi.org/10.1371/journal.pone.0112610.

Garcin, Y., Schwab, V.F., Gleixner, G., Kahmen, A., Todou, G., Séné, O., Onana, J.M., Achoundong, G., Sachse, D., 2012. Hydrogen isotope ratios of lacustrine sedimentary n-alkanes as proxies of tropical African hydrology: Insights from a calibration transect across Cameroon. Geochimica et Cosmochimica Acta 79, 106–126. https://doi.org/10.1016/j.gca.2011.11.039.

Garcin, Y., Schefuß, E., Schwab, V.F., Garreta, V., Gleixner, G., Vincens, A., Todou, G., Séné, O., Onana, J.M., Achoundong, G., Sachse, D., 2014. Reconstructing C_3 and C_4 vegetation cover using n-alkane carbon isotope ratios in recent lake sediments from Cameroon, Western Central Africa. Geochimica et Cosmochimica Acta 142, 482–500. https://doi.org/10.1016/j.gca.2014.07.004.

Gieske, A., 1997. Modelling outflow from the Jao/Boro River system in the Okavango Delta, Botswana. Journal of Hydrology 193, 214–239. https://doi.org/10.1016/S0022-1694(96)03147-2.

Gondwe, M.J., Helfter, C., Murray-Hudson, M., Levy, P.E., Mosimanyana, E., Makati, A., Mfundisi, K.B., Skiba, U.M., 2021. Methane flux measurements along a floodplain soil moisture gradient in the Okavango Delta, Botswana. Philosophical Transactions of the Royal Society A: Mathematical, Physical and Engineering Sciences 379. https://doi.org/10.1098/rsta.2020.0448.

Gondwe, M.J., Masamba, W.R., 2014. Spatial and temporal dynamics of diffusive methane emissions in the Okavango Delta, northern Botswana, Africa. Wetlands ecology and management 22, 63–78. https://doi.org/10.1007/s11273-013-9323-5.

Griepentrog, M., De Wispelaere, L., Bauters, M., Bodé, S., Hemp, A., Verschuren, D., Boeckx, P., 2019. Influence of plant growth form, habitat and season on leaf-wax n-alkane hydrogen-isotopic signatures in equatorial East Africa. Geochimica et Cosmochimica Acta 263, 122–139. https://doi.org/10.1016/j.gca.2019.08.004.

Gumbricht, T., McCarthy, J., McCarthy, T.S., 2004. Channels, wetlands and islands in the Okavango Delta, Botswana, and their relation to hydrological and sedimentological processes. Earth Surface Processes and Landforms 29, 15–29. https://doi.org/10.1002/esp.1008.

Heinzelmann, S.M., Villanueva, L., Sinke-Schoen, D., Sinninghe Damsté, J.S., Schouten, S., Van der Meer, M.T., 2015. Impact of metabolism and growth phase on the hydrogen isotopic composition of microbial fatty acids. Frontiers in Microbiology 6, 408. https://doi.org/10.3389/fmicb.2015.00408.

Heath, R., Heath, A. (2009). Field guide to the plants of Northern Botswana including the Okavango Delta (pp. vi+-593). ISSN 978-1-84246-183-9.

Hou, J., D'Andrea, W.J., MacDonald, D., Huang, Y., 2007. Evidence for water use efficiency as an important factor in determining the δD values of tree leaf waxes. Organic Geochemistry 38, 1251–1255. https://doi.org/10.1016/j.orggeochem.2007.03.011.

Huang, Y., Shuman, B., Wang, Y., Webb, T., 2004. Hydrogen isotope ratios of individual lipids in lake sediments as novel tracers of climatic and environmental change: a surface sediment test. Journal of Paleolimnology 31, 363–375. https://doi.org/10.1023/B:JOPL.0000021855.80535.13.

Inman, V.L., Lyons, M.B., 2020. Automated inundation mapping over large areas using Landsat Data and Google Earth Engine. Remote Sensing 12, 8. https://doi.org/10.3390/rs12081348.

Jolivet, M., Dauteuil, O., Dia, A., Davranche, M., Pierson-Wickmann, A.-C., Barrier, L., Murray-Hudson, M., Mazrui, N., Marsac, R., Cheng, F., Li, X., 2023. Highly contrasted geochemical pattern in sediments of the Okavango Delta, Botswana driven by dust supply, hydrological heritage and biogeochemical reactions. Geochemistry, Geophysics, Geosystems 24, e2023GC010978. https://doi.org/10.1029/2023GC010978.

Kristen, I., Wilkes, H., Vieth, A., Zink, K.-G., Plessen, B., Thorpe, J., Partridge, T.C., Oberhänsli, H., 2010. Biomarker and stable carbon isotope analyses of sedimentary organic matter from Lake Tswaing: evidence for deglacial wetness and early Holocene drought from South Africa. Journal of Paleolimnology 44, 143–160. https://doi.org/10.1007/s10933-009-9393-9.

Krull, E., Sachse, D., Mügler, I., Thiele, A., Gleixner, G., 2006. Compound-specific δ13C and δ2H analyses of plant and soil organic matter: a preliminary assessment of the effects of vegetation change on ecosystem hydrology. Soil Biology and Biochemistry 38, 3211–3221. https://doi.org/10.1016/j.soilbio.2006.04.008.

Lattaud, J., Bröder, L., Haghipour, N., Rickli, J., Giosan, L., Eglinton, T.I., 2021. Influence of hydraulic connectivity on carbon burial efficiency in Mackenzie Delta Lake sediments. Journal of Geophysical Research: Biogeosciences 126. https://doi.org/10.1029/2020jg006054.

Liu, J., Liu, W., An, Z., Yang, H., 2016. Different hydrogen isotope fractionations during lipid formation in higher plants: implications for paleohydrology reconstruction at a global scale. Scientific Reports 6, 1. https://doi.org/10.1038/srep19711.

Lourenco, M., Woodborne, S., 2023. Defining the Angolan Highlands Water Tower, a 40 plus-year precipitation budget of the headwater catchments of the Okavango Delta. Environmental Monitoring and Assessment 195, 859. https://doi.org/10.1007/s10661-023-11448-7.

Lubinda, A.K., 2012. Transpiration in Various Riparian Woodland Species of the Okavango Delta. University of Botswana, Botswana.

Magill, C.R., Eglinton, G., Eglinton, T.I., 2019. Isotopic variance among plant lipid homologues correlates with biodiversity patterns of their source communities. PLoS One 14, e0212211. https://doi.org/10.1371/journal.pone.0212211.

Mantlana, K.B., Arneth, A., Veenendaal, E.M., Wohland, P., Wolski, P., Kolle, O., Lloyd, J., 2008. Photosynthetic properties of C4 plants growing in an African savanna/wetland mosaic. Journal of experimental botany 59 (14), 3941–3952. https://doi.org/10.1093/jxb/ern237.

Martins-Loução, M.A., Wollenweber, B., Raven, J.A., 1993. Response of Salvinia spp. to different nitrogen sources: the acid-base regulation approach. Oecologia 93, 524–530. https://doi.org/10.1007/BF00328961.

Matsumoto, K., Kawamura, K., Uchida, M., Shibata, Y., 2007. Radiocarbon content and stable carbon isotopic ratios of individual fatty acids in subsurface soil: implication for selective microbial degradation and modification of soil organic matter. Geochemical Journal 41, 483–492. https://doi.org/10.2343/geochemj.41.483.

McCarthy, T.S., Ellery, W.N., 1998. The Okavango Delta. Transactions of the Royal Society of South Africa 53, 157–182. https://doi.org/10.1080/00359199809520384.

McIntyre, C., Wacker, L., Haghipour, N., Blattmann, T.M., Fahrni, S., Usman, M.O., Eglinton, T.I., Synal, H.-A., 2016. Online ^{13}C and ^{14}C gas measurements by EA-IRMS–AMS at ETH Zürich. Radiocarbon 59, 893–903.

Milzow, C., Kgotlhang, L., Bauer-Gottwein, P., Meier, P., Kinzelbach, W., 2009. Regional review: The hydrology of the Okavango Delta, Botswana—processes, data and modelling. Hydrogeology Journal 17, 1297–1328. https://doi.org/10.1007/s10040-009-0436-0.

Mooney, H.A., Troughton, J.H., Berry, J.A., 1977. Carbon isotope ratio measurements of succulent plants in southern Africa. Oecologia 30, 295–305. https://doi.org/10.1007/BF00399762.

Mosepele, K., Kolding, J., Bokhutlo, T., Mosepele, B.Q., Molefe, M., 2022. The Okavango Delta: fisheries in a fluctuating floodplain system. Frontiers in Environmental Science 10. doi: 10.3389/fenvs.2022.854835.

Naafs, D.F., van Bergen, P.F., Boogert, S.J., de Leeuw, J.W., 2004. Solvent-extractable lipids in an acid andic forest soil; variations with depth and season. Soil Biology and Biochemistry 36 (2), 297–308. https://doi.org/10.1016/j.soilbio.2003.10.005.

Osborne, C.P., Sack, L., 2012. Evolution of C_4 plants: a new hypothesis for an interaction of CO2 and water relations mediated by plant hydraulics. Philosophical Transactions of the Royal Society B: Biological Sciences 367, 583–600. https://doi.org/10.1098/rstb.2011.0261.

Pires, T.P., dos Santos Souza, E., Kuki, K.N., Motoike, S.Y., 2013. Ecophysiological traits of the macaw palm: a contribution towards the domestication of a novel oil crop. Industrial Crops and Products 44, 200–210. https://doi.org/10.1016/j.indcrop.2012.09.029.

Ramberg, L., Wolski, P., Krah, M., 2006. Water balance and infiltration in a seasonal floodplain in the Okavango Delta, Botswana. Wetlands 26, 677–690. https://doi.org/10.1672/0277-5212(2006)26[677:WBAIIA]2.0.CO;2.

Reiffarth, D.G., Petticrew, E.L., Owens, P.N., Lobb, D.A., 2016. Sources of variability in fatty acid (FA) biomarkers in the application of compound-specific stable isotopes (CSSIs) to soil and sediment fingerprinting and tracing: a review. Science of the Total Environment 565, 8–27. https://doi.org/10.1016/j.scitotenv.2016.04.137.

Ritchie, R., 2012. Photosynthesis in the blue water lily (*Nymphaea caerulea Saligny*) using pulse amplitude modulation fluorometry. International Journal of Plant Sciences 172, 124–136. https://doi.org/10.1086/663168.

Rommerskirchen, F., Plader, A., Eglinton, G., Chikaraishi, Y., Rullkötter, J., 2006. Chemotaxonomic significance of distribution and stable carbon isotopic composition of long-chain alkanes and alkan-1-ols in C_4 grass waxes. Organic Geochemistry 37, 1303–1332. https://doi.org/10.1016/j.orggeochem.2005.12.013.

Sachse, D., Radke, J., Gleixner, G., 2004. Hydrogen isotope ratios of recent lacustrine sedimentary n-alkanes record modern climate variability. Geochimica et Cosmochimica Acta 68, 4877–4889. https://doi.org/10.1016/j.gca.2004.06.004.

Sachse, D., Billault, I., Bowen, G.J., Chikaraishi, Y., Dawson, T.E., Feakins, S.J., Freeman, K.H., Magill, C.R., McInerney, F.A., van der Meer, M.T.J., Polissar, P., Robins, R.J., Sachs, J.P., Schmidt, H.-L., Sessions, A.L., White, J.W.C., West, J.B., Kahmen, A., 2012. Molecular paleohydrology: Interpreting the hydrogen-isotopic composition of lipid biomarkers from photosynthesizing organisms. Annual Review of Earth and Planetary Sciences 40, 221–249. https://doi.org/10.1146/annurev-earth-042711-105535.

Sauer, P.E., Eglinton, T.I., Schimmelmann, A., Hayes, J.M., Sessions, A.L., 2001. Compound-specific D/H ratios of lipid biomarkers from sediments as a proxy for environmental and climatic conditions. Geochimica et Cosmochimica Acta 65, 213–222. https://doi.org/10.1016/s0016-7037(00)00520-2.

Saurer, M., Borella, S., Leuenberger, M., 1997. $\Delta^{18}O$ of tree rings of beech (Fagus silvatica) as a record of $\delta^{18}O$ of the growing season precipitation. Tellus B: Chemical and Physical Meteorology 49, 80–92. https://doi.org/10.3402/tellusb.v49i1.15952.

Schwab, V.F., Garcin, Y., Sachse, D., Todou, G., Séné, O., Onana, J.-M., Achoundong, G., Gleixner, G., 2015. Effect of aridity on $\delta^{13}C$ and δD values of C_3 plant- and C_4 graminoid-derived leaf wax lipids from soils along an environmental gradient in Cameroon (Western Central Africa). Organic Geochemistry 78, 99–109. https://doi.org/10.1016/j.orggeochem.2014.09.007.

Sessions, A.L., Burgoyne, T.W., Schimmelmann, A., Hayes, J.M., 1999. Fractionation of hydrogen isotopes in lipid biosynthesis. Organic Geochemistry 30, 1193–1200. https://doi.org/10.1016/S0146-6380(99)00094-7.

Singarayer, J.S., Burrough, S.L., 2015. Interhemispheric dynamics of the African rainbelt during the late Quaternary. Quaternary Science Reviews 124, 48–67. https://doi.org/10.1016/j.quascirev.2015.06.021.

Snyder, K.A., Williams, D.G., 2000. Water sources used by riparian trees varies among stream types on the San Pedro River. Arizona. Agricultural and Forest Meteorology 105 (1–3), 227–240. https://doi.org/10.1016/S0168-1923(00)00193-3.

Sutcliff, J.V., Parks, Y.P., 1989. Comparative water balances of selected African wetlands. Hydrological Sciences Journal 34, 49–62. https://doi.org/10.1080/02626668909491308.

Thomas, D., 2019. Quaternary Climate Variation in Southern Africa. Oxford Research Encyclopedia of Climate. Science. https://oxfordre.com/climatescience/view/10.1093/acrefore/9780190228620.001.0001/acrefore-9780190228620-e-527 Retrieved 8 Jul. 2024, from.

Vähätalo, A.V., Wetzel, R.G., 2008. Long-term photochemical and microbial decomposition of wetland-derived dissolved organic matter with alteration of ^{13}C:^{12}C mass ratio. Limnology and Oceanography 53, 1387–1392. https://doi.org/10.4319/lo.2008.53.4.1387.

Vogts, A., Moossen, H., Rommerskirchen, F., Rullkötter, J., 2009. Distribution patterns and stable carbon isotopic composition of alkanes and alkan-1-ols from plant waxes of African rain forest and savanna C3 species. Organic Geochemistry 40, 1037–1054. https://doi.org/10.1016/j.orggeochem.2009.07.011.

Werth, M., Kuzyakov, Y., 2010. 13C fractionation at the root–microorganisms–soil interface: a review and outlook for partitioning studies. Soil Biology and Biochemistry 42, 1372–1384. https://doi.org/10.1016/j.soilbio.2010.04.009.

West, A.G., Patrickson, S.J., Ehleringer, J.R., 2006. Water extraction times for plant and soil materials used in stable isotope analysis. Rapid Communications in Mass Spectrometry 20, 1317–1321. https://doi.org/10.1002/rcm.2456.

Wijker, R.S., Sessions, A.L., Fuhrer, T., Phan, M., 2019. 2H/1H variation in microbial lipids is controlled by NADPH metabolism. Proceedings of the National Academy of Sciences 116 (25), 12173–12182. https://doi.org/10.1073/pnas.18183721.